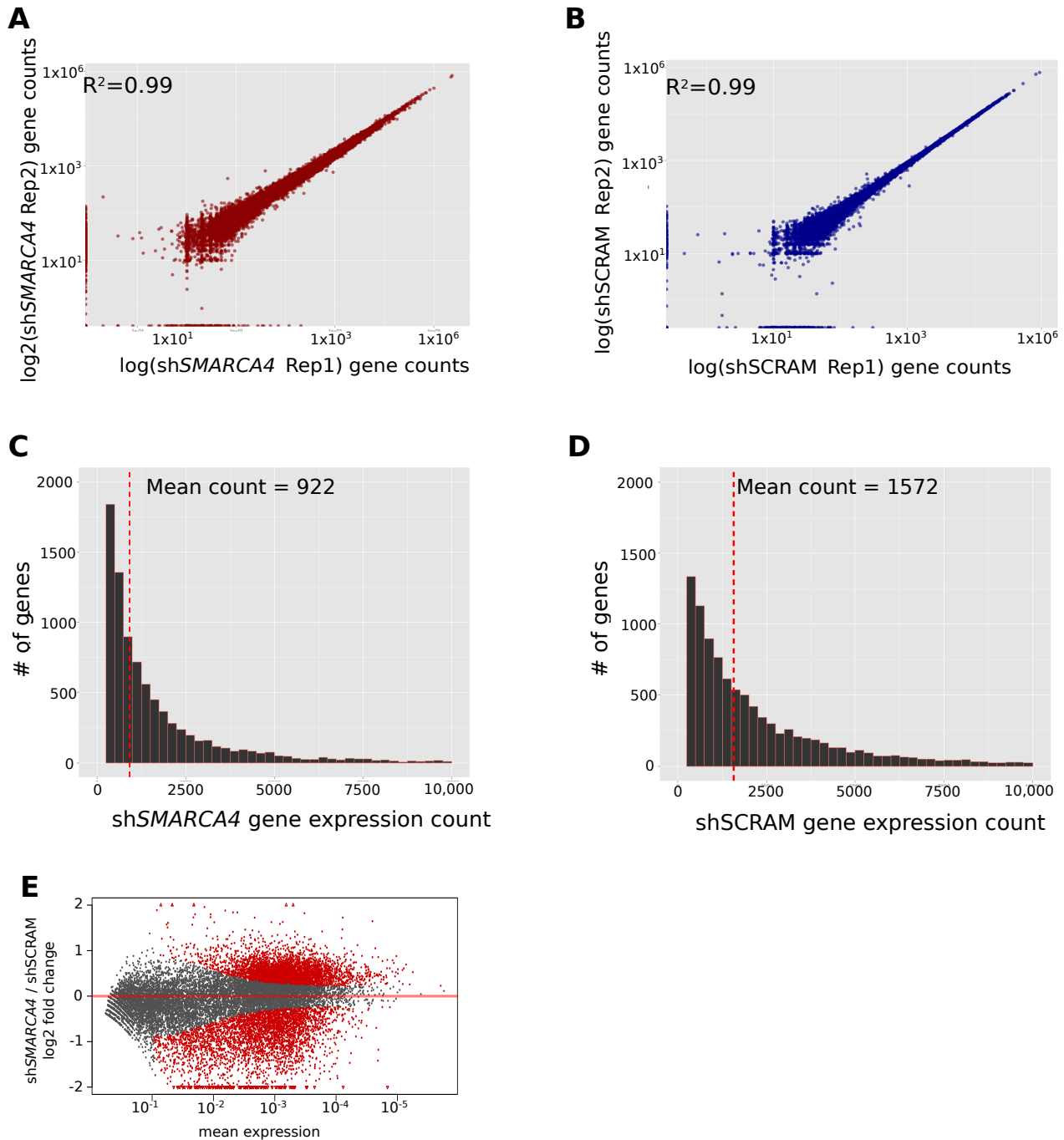


Supplementary Figure S1



Supplementary Figure S1 - RNAseq Analysis in SMARCA4 knockdown cells:

Scatterplots showing the gene expression Pearson Correlation coefficients

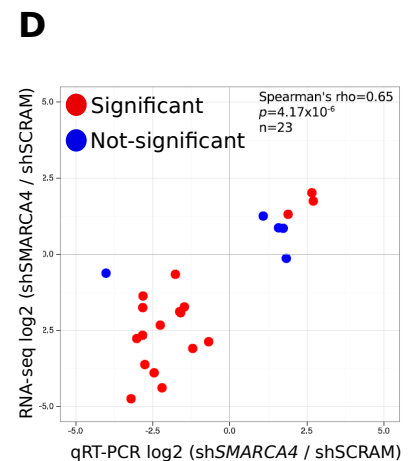
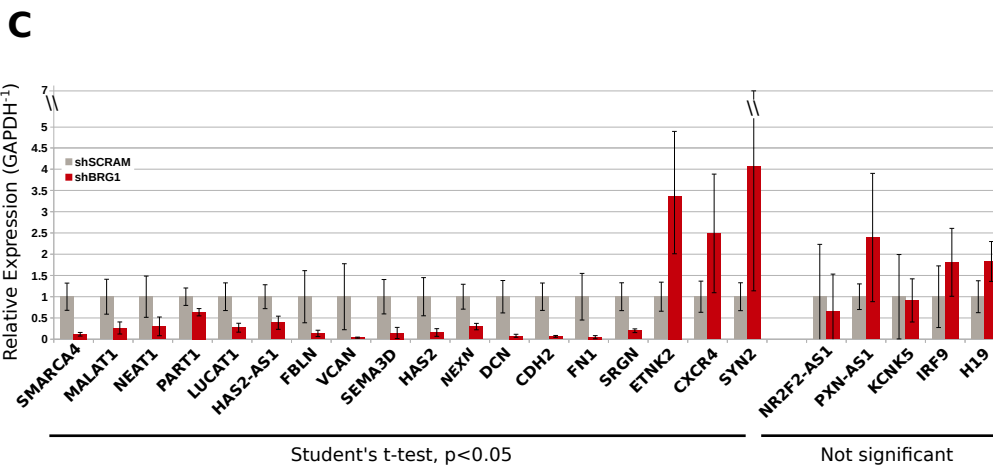
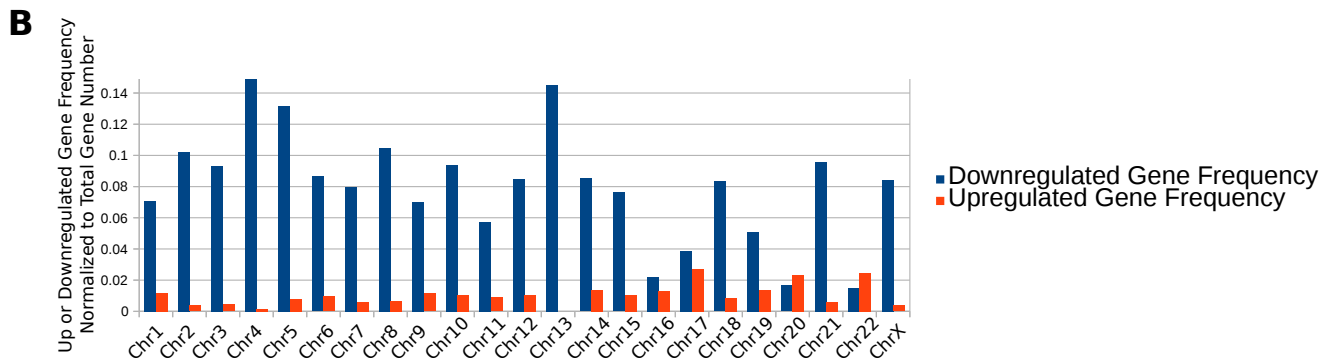
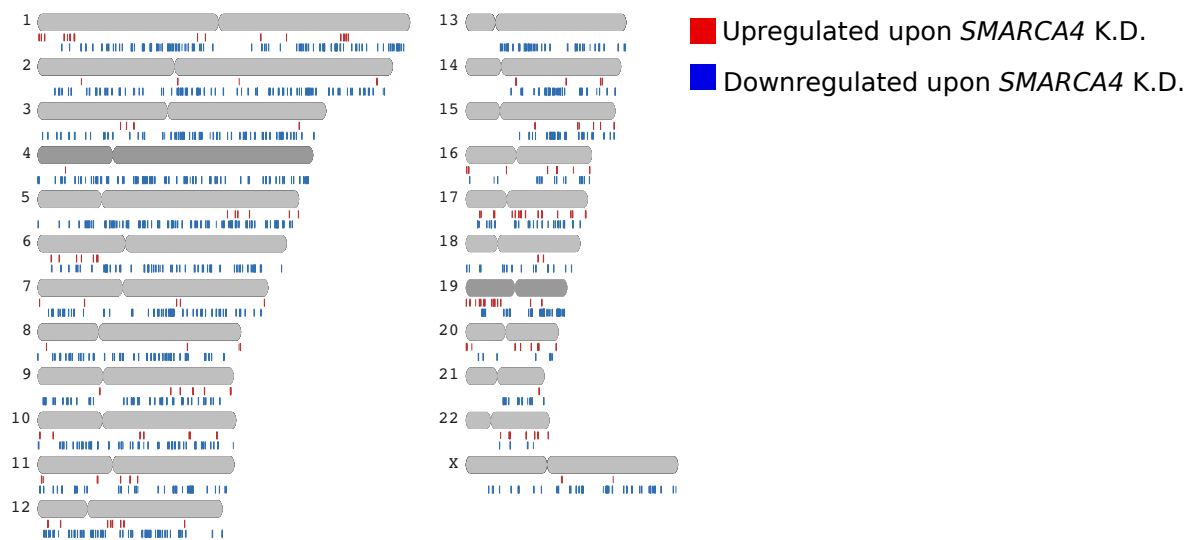
between the RNA-seq biological replicates for **A)** shSMARCA4 and **B)** shSCRAM samples.

Histograms showing the number of genes and the expression levels for **C)** shSMARCA4 and **D)** shSCRAM combined datasets. SMARCA4 depletion results in a lower mean gene expression.

E) MA-plot showing the log₂ fold change and the mean expression of significantly altered (red) and unaltered genes (black).

Supplementary Figure S2

A MCF-10A shSMARCA4/shSCRAM Differentially Expressed Gene Positions



Supplementary Figure S2 - Validation of RNA-seq Analysis

A) Chromosome ideograms showing the locations of up (red) and down (blue) regulated genes upon *SMARCA4* knockdown.

B) Bar graph showing the gene frequencies of up (red) and down (blue) regulated genes for each chromosome.

C) qRT-PCR validation of the RNA-seq data for 23 genes. The y-axis shows the relative expression level of each gene compared to GAPDH. 18 of 23 genes showed significant differential expression. Error bars: S.D.

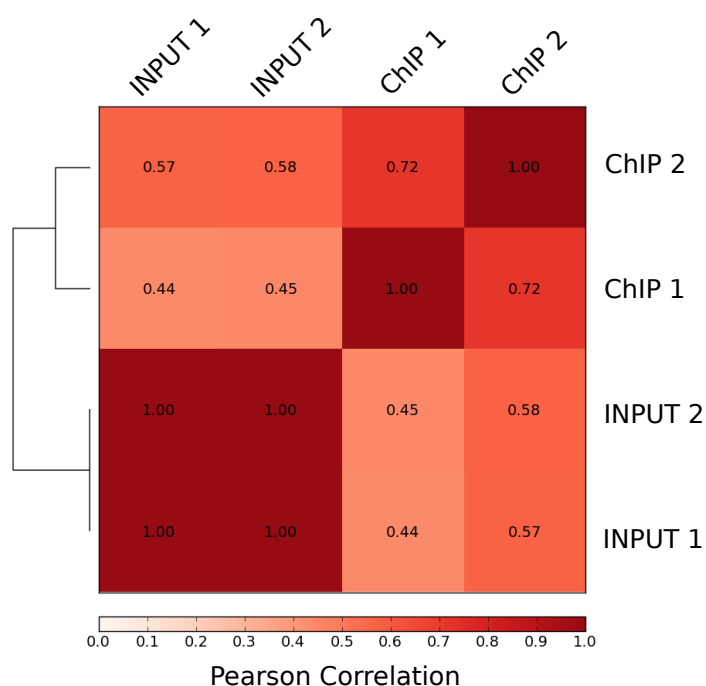
D) Scatterplot showing the correlation of log₂ fold change values for the 23 genes from the RNA-seq and qRT-PCR analyses. There is a significant positive correlation between the RNA-seq and qRT-PCR data (Spearman's $\rho = 0.65$).

Supplementary Figure S3

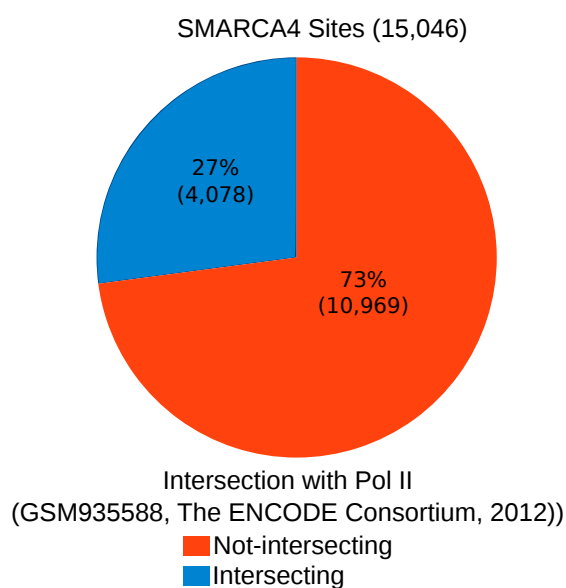
A

Sample Name	Biological Replicate	Raw Reads	Mapped Reads
SMARCA4 ChIP 1	1	14,642,947	9,057,272
SMARCA4 ChIP 2	2	25,641,108	20,088,204
INPUT 1	1	25,624,664	22,301,264
INPUT 2	2	37,688,445	32,712,701

B



C



Supplementary Figure S3 - SMARCA4 ChIP-seq Analysis

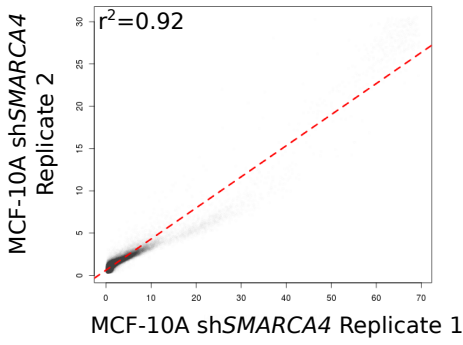
A) Table showing the sequenced and mapped reads for each ChIP-seq biological replicate.

B) Matrix showing the Pearson correlation of the signal intensity between the pull down (ChIP) and input samples.

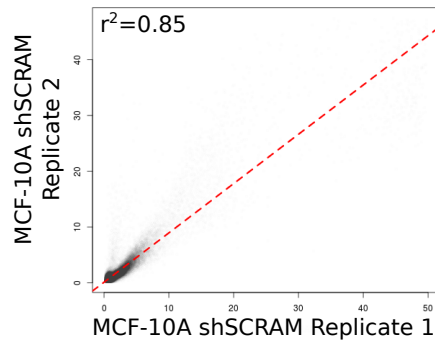
C) Pie chart showing intersections of SMARCA4 peaks with publicly available Pol2 peaks from MCF-10A cells.

Supplementary Figure S4

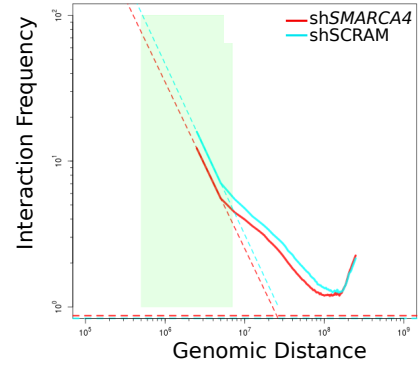
A



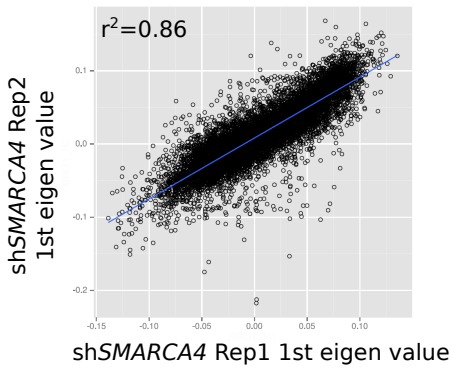
B



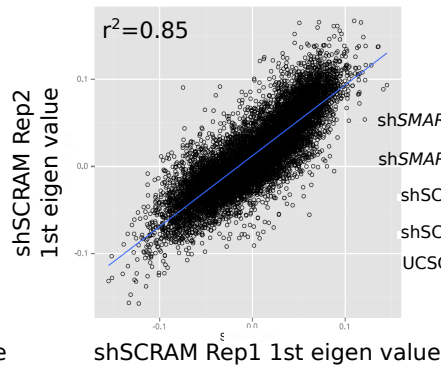
C



D

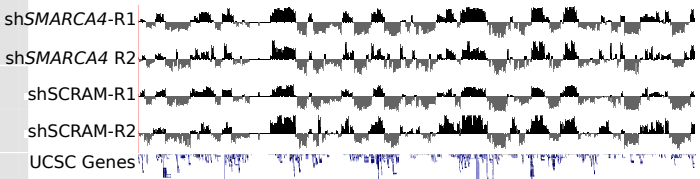


E

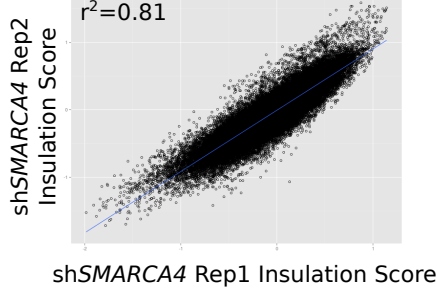


F

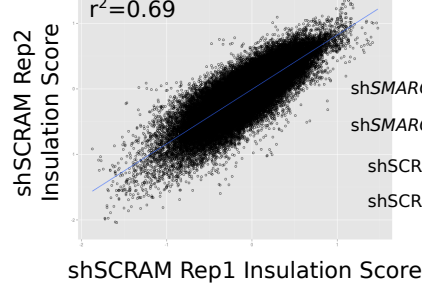
Compartment Profile (1st eigen vector)
Chr18



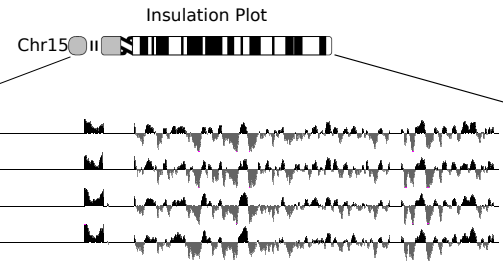
G



H



I

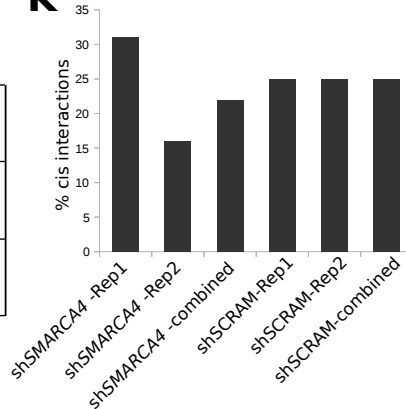


J

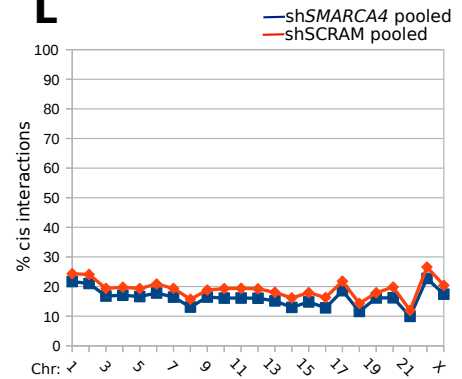
Pearson Correlation Between Pooled Replicates (r^2)

shSCRAM vs. shSMARCA4	0.968
shSCRAM vs parental (Barutcu et al. 2015)	0.919
shSMARCA4 vs parental (Barutcu et al. 2015)	0.946

K



L



Supplementary Figure S4 - Reproducibility of Hi-C Experiments

A-B) Scatter plots comparing normalized interactions between pairs of 2.5Mb bins in the two biological replicates from **A)** shSMARCA4 and **B)** shSCRAM datasets. Pearson correlation (r^2 value) is shown on the graphs.

C) Scaling plot at 2.5Mb resolution showing that in both shSMARCA4 and shSCRAM Hi-C samples, interaction frequency decreases similarly as a function of genomic distance. The difference between the shSMARCA4 and shSCRAM curves is due to the differences in % cis interactions.

D-E) Scatter plots showing the correlation of the 1st eigenvector values for each 250kb bin from the compartment analysis for each biological replicate in **D)** shSMARCA4 and **E)** shSCRAM datasets.

F) Example of the first eigen values for each biological replicate across Chr18. The replicates show high correlation in genomic compartmentalization.

G-H) Insulation score correlation among the biological replicates for each 40kb bin for **G)** shSMARCA4 and **H)** shSCRAM datasets.

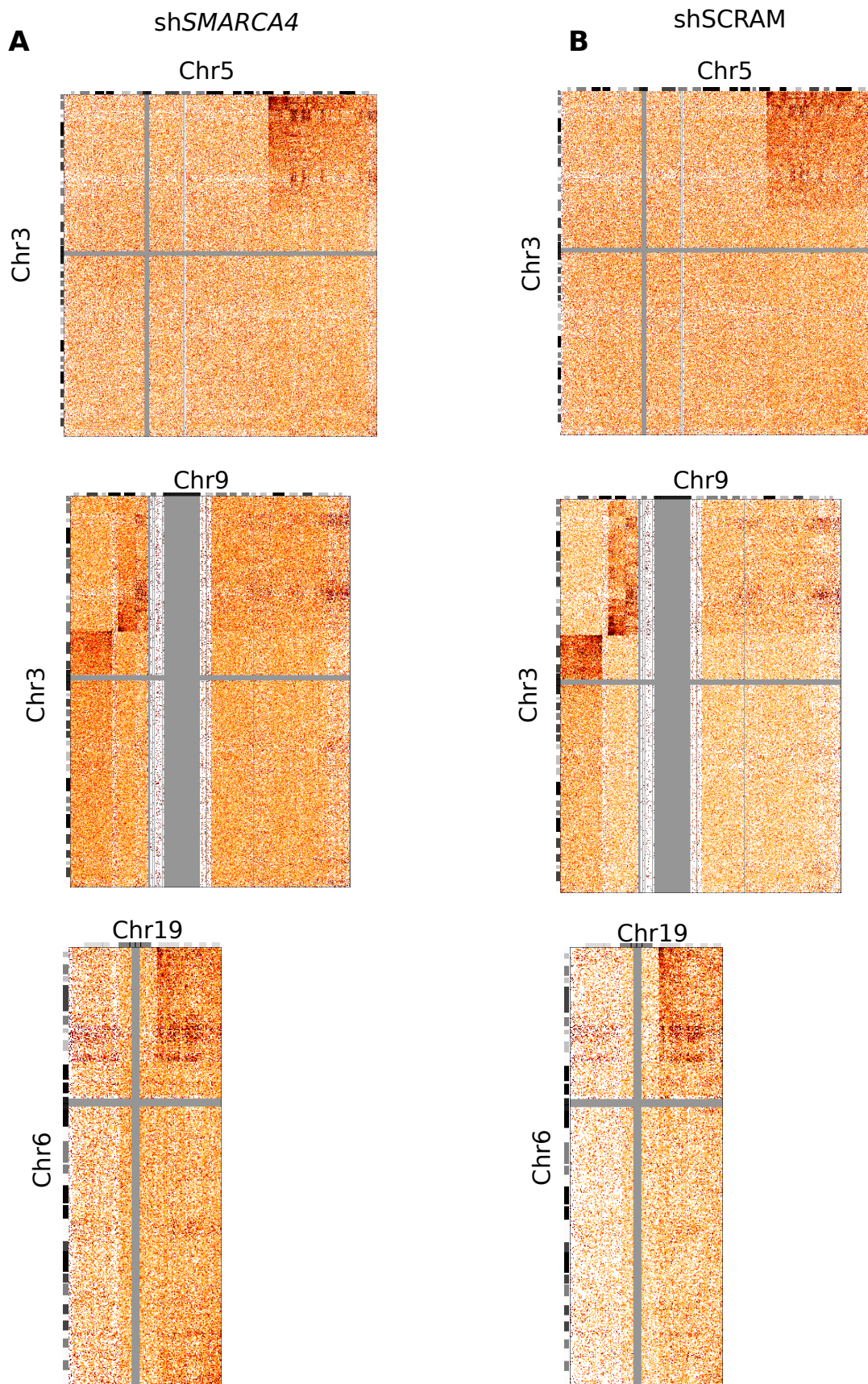
I) Example of the insulation plot across Chr15 for each biological replicate.

J) Pearson correlations of the pooled Hi-C replicates between shSCRAM, shSMARCA4, and previously published parental (wildtype) MCF-10A cells (Barutcu et al. 2015).

K) Bargraph showing the cis interaction percentage of individual and pooled shSMARCA4 and shSCRAM Hi-C replicates.

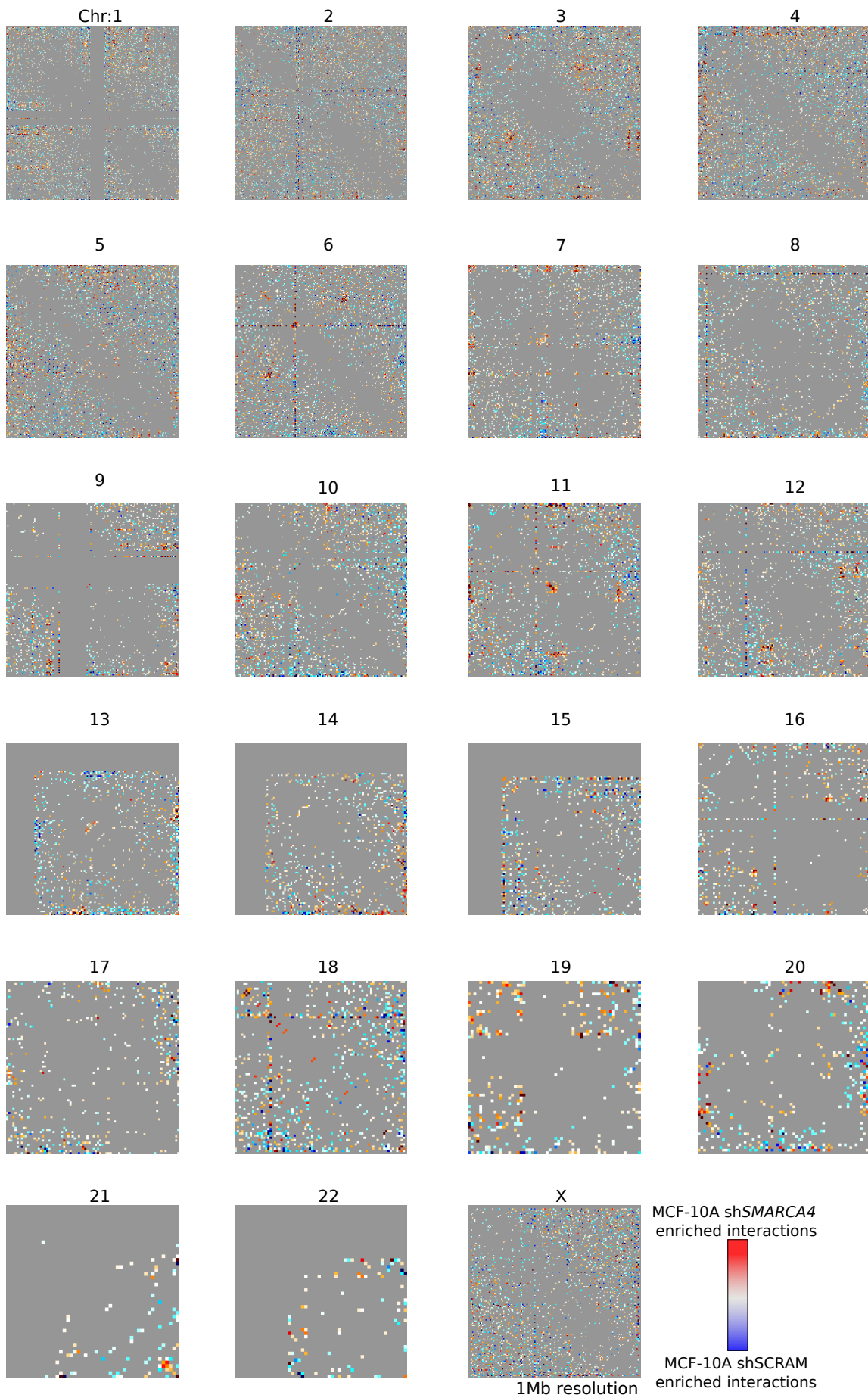
L) The percentage of cis/trans interaction frequencies of pooled shSMARCA4 and shSCRAM datasets for each chromosome.

Supplementary Figure S5



Supplementary Figure S5 - Translocations in shSCRAM and shSMARCA4 MCF-10A cells
Inter-chromosomal interaction heatmaps showing the translocated regions in the MCF-10A genome for **A)** shSMARCA4 and **B)** shSCRAM Hi-C datasets.

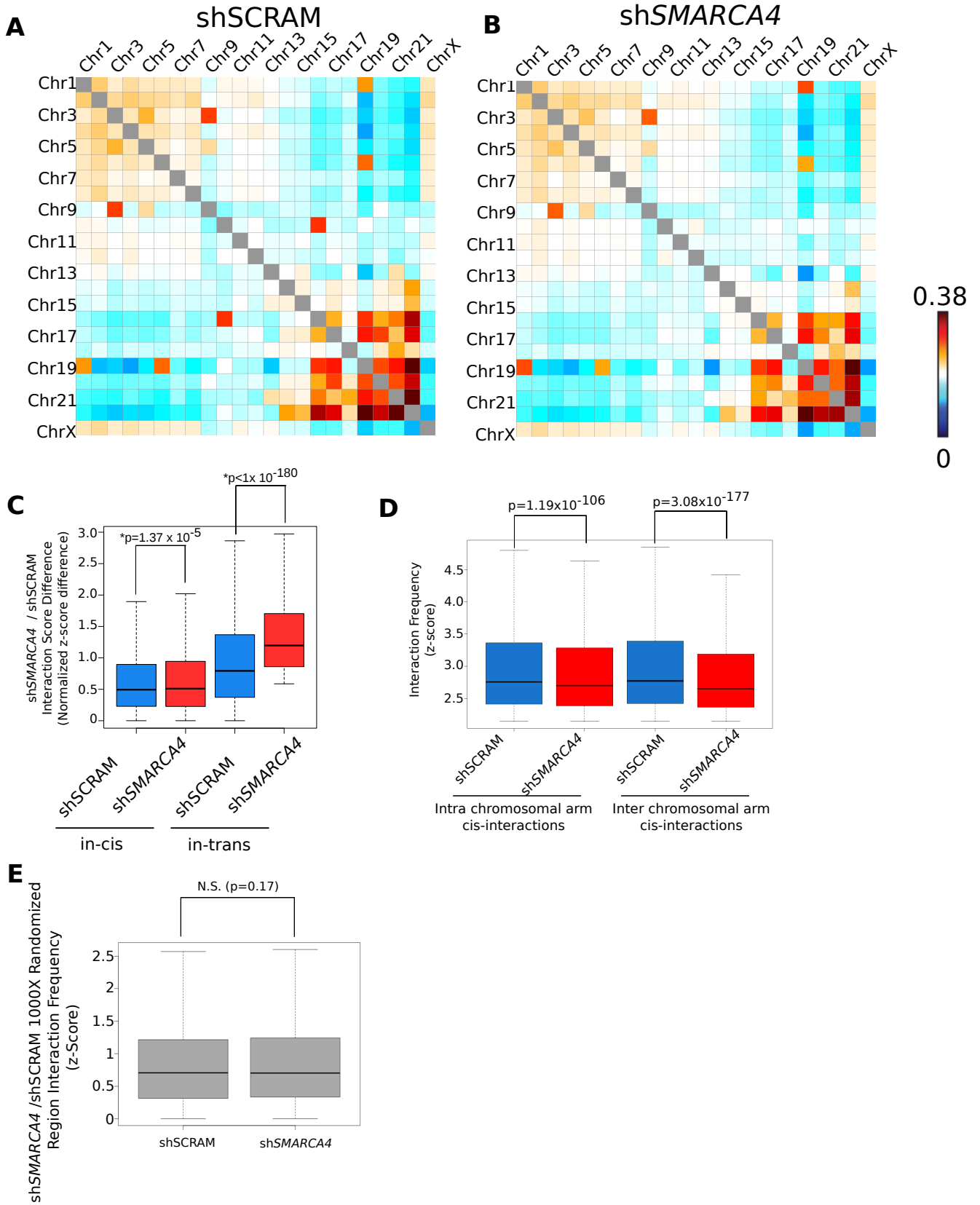
Supplementary Figure S6



Supplementary Figure S6 - SMARCA4-dependent significant interactions

shSMARCA4 / shSCRAM interactions that are significantly different (see Methods) at 1Mb for each chromosome (versus itself).

Supplementary Figure S7



Supplementary Figure S7 - Large scale alterations in *SMARCA4* knockdown cells

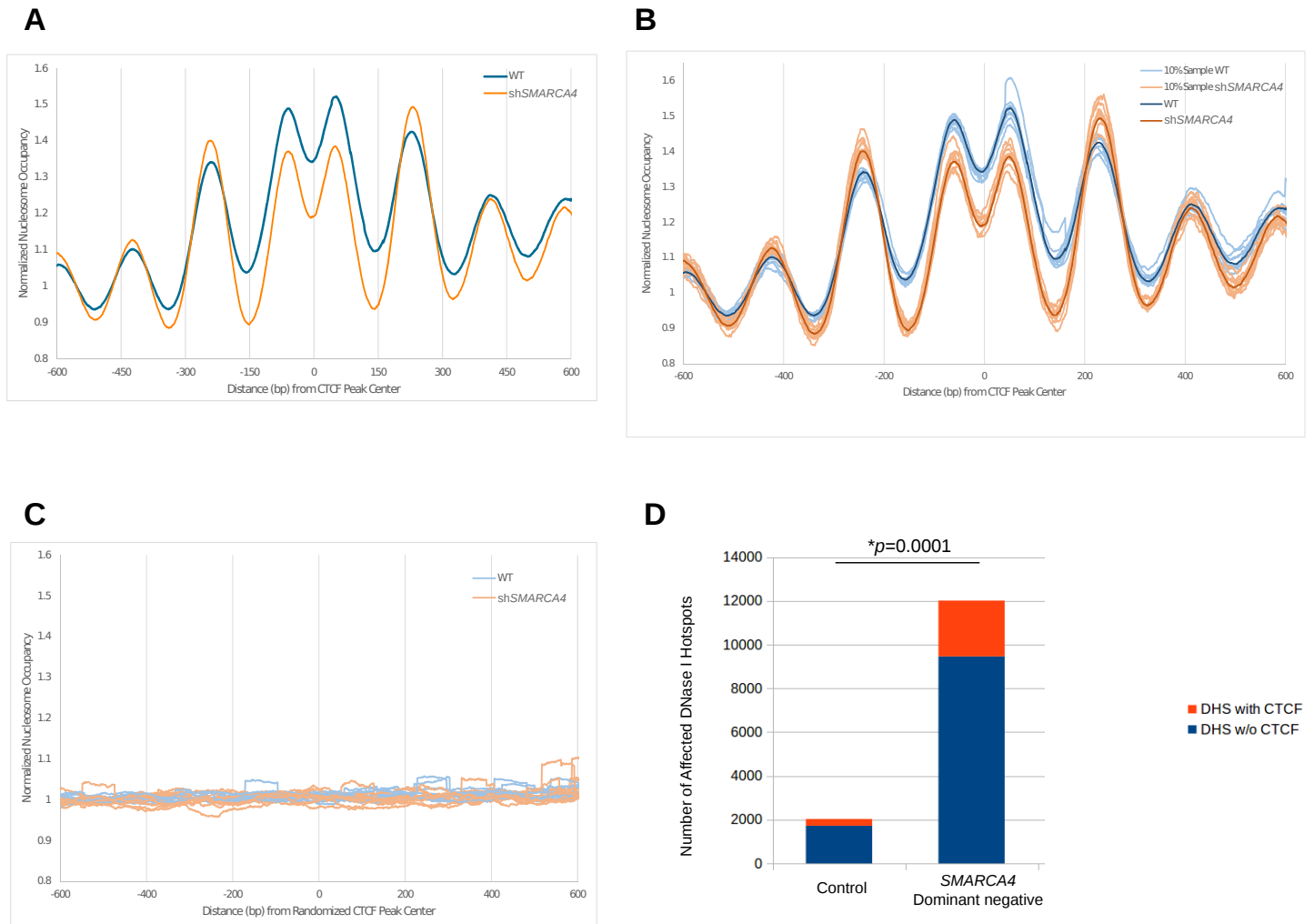
Chromosome by chromosome interaction heatmaps for **A)** shSCRAM and **B)** sh*SMARCA4* Hi-C datasets.

C) Boxplot showing the sh*SMARCA4* / shSCRAM interaction difference scores for cis and trans-interactions. sh*SMARCA4* MCF-10A cells show higher frequency of trans-interactions (Replicate Pearson correlation $r^2=0.94$ for sh*SMARCA4* and $r^2=0.85$ for shSCRAM biological replicates.)

D) Boxplot showing the intra-arm and inter-arm chromosomal interaction frequencies for sh*SMARCA4* and shSCRAM datasets. p-values: Wilcoxon rank-sum test.

E) 1000X randomized set of regions to serve as a control for telomeric interactions. p-values: Wilcoxon rank-sum test.

Supplementary Figure S9



SMARCA4 knockdown affects the nucleosome occupancy and chromatin accessibility near CTCF sites.

A) Plot showing the nucleosome occupancy around the CTCF sites in wildtype and *SMARCA4* knockdown cells. MNase-seq data from wildtype and *SMARCA4* knockdown MEFs (Tolstorukov et al, 2013) were used. The MEF CTCF ChIP-seq data was downloaded from the ENCODE project (ENCFF001YAQ). Nucleosome occupancy was computed for each CTCF site by adding the nucleosome tag counts in 75 bp windows with 1bp smoothing step from the peak center of the CTCF sites, and normalizing the resulting score by the average tag count (positions from -1kb to -0.7 kb from the CTCF site).

B) Results of repeated random subsampling of 10% of the CTCF sites (light colored traces) superimposed on the results for the full dataset (dark lines), showing that the *SMARCA4*-dependent decrease in nucleosome occupancy around CTCF sites is not due to a few outlier sites harboring an unusual decrease.

C) Randomization of the MNase-seq signal by randomly shifting the CTCF site positions 2 to 100kb up or downstream. There is no significant pattern or difference between WT and mutant MNase-seq signals.

D) Bar graph showing *SMARCA4*-dependent altered DNase I hypersensitivity near CTCF sites. Changes in chromatin accessibility (Morris et al. 2014) were determined by calculating the Tet+/Tet- tag density values of each DNase I hotspot in the control and *SMARCA4* dominant negative expressing 3134 murine epithelial cells. The hotspots with a Tet+/Tet- ratio more than +/- 1 standard deviation of the average ratio from all the hotspots were considered as "affected". The affected sites were intersected with the CTCF ChIP-seq dataset from the same cell lines (Stavreva et al. 2015). The *SMARCA4*-DN affected DNase I sites overlap significantly more with CTCF sites (Chi-square Test with Yates' correction) compared to control cells.